Binary Two-Dimensional Honeycomb Lattice with Strong Spin-Orbit Coupling and Electron-Hole Asymmetry

Jian Gou,[1,2] Bingyu Xia,[3,4] Hang Li,[1,2] Xuguang Wang,[1,2] Longjuan Kong,[1,2] Peng Cheng,[1,3]
Hui Li,[5] Weifeng Zhang,[9] Tian Qian,[1] Hong Ding,[1] Yong Xu,[3,4,7,,*]
Wenhui Duan,[3,4,8] Kehui Wu,[1,2,4,6,†] and Lan Chen[1,2,6,‡]

[1]*Institute of Physics, Chinese Academy of Sciences, Beijing 100190, China*
[2]*School of Physics, University of Chinese Academy of Sciences, Beijing 100049, China*
[3]*State Key Laboratory of Low-Dimensional Quantum Physics, Department of Physics, Tsinghua University, Beijing 100084, China*
[4]*Collaborative Innovation Center of Quantum Matter, Beijing 100084/100871, China*
[5]*Beijing Advanced Innovation Center for Soft Matter Science and Engineering, Beijing University of Chemical Technology, Beijing 100029, China*
[6]*CAS Center for Excellence in Topological Computation, University of Chinese Academy of Sciences, Beijing 1000190, China*
[7]*RIKEN Center for Emergent Matter Science (CEMS), Wako, Saitama 351-0198, Japan*
[8]*Institute for Advanced Study, Tsinghua University, Beijing 100084, China*
[9]*School of Physics and Electronics, Henan University, Kaifeng 475004, Henan Province, China*

Two-dimensional (2D) materials consisting of heavy atoms with particular arrangements may host exotic quantum properties. Here, we report a unique 2D semiconducting binary compound, a Sn_2Bi atomic layer on Si(111), in which hexagons are formed by bonding Bi with a triangular network of Sn. Because of the unique honeycomb configuration, the heavy elements, and the energy-dependent hybridization between Sn and Bi, 2D Sn_2Bi not only shows strong spin-orbit coupling effects but also exhibits high electron-hole asymmetry: Nearly free hole bands and dispersionless flat electron bands coexist in the same system. By tuning the Fermi level, it is possible to preserve both nearly free and strongly localized charge carriers in the same 2D material, which provides an ideal platform for the studies of strongly correlated phenomena and possible applications in nanodevices.

The exploration of novel two-dimensional (2D) materials has attracted enormous research effort since the discovery of graphene [1,2], due to their promising properties and potential applications. Recently, the material family has been significantly enriched by adding a series of new members hosting diverse 2D quantum phases, including topology [3–5], ferromagnetism [6,7], ferroelectricity [8], charge density wave [9], superconductivity [10], etc. Current research predominantly focuses on 2D layered (like transition metal dichalcogenides [11]) or elemental (like graphyne [12], silicene [13–15], germanene [16,17], stanene [18,19], borophene [20,21], blue phosphorous [22,23], antimonene [24], and bismuthene [25]) materials or others (like 2D alkali-earth metal hydroxides [26], graphene oxides, and silicene oxides [27–28]). In contrast, nonlayered binary compounds in the 2D limit could possess unusual chemical stoichiometry and atomic configuration and display extraordinary electronic properties, which greatly expands the opportunities for future research. This broad class of 2D materials, however, remains largely unexplored.

The development of new 2D nonlayered materials with high quality requires fine control of the growth dynamics at the atomic scale and, thus, represents a grand challenge to the research community. In practice, the fabrication and application of 2D materials both need a supporting substrate. Semiconducting substrates are usually preferable, as they enable the measurement of optical and transport properties within the substrate band gap. The exploration of novel 2D atomic layers on a silicon substrate is of particular interest, since it could be immediately applicable in the silicon industry. One intriguing direction is novel 2D binary materials composed of heavy elements, with strong spin-orbit coupling (SOC) effects and crystallized in a honeycomb lattice—a fascinating model lattice displaying exotic quantum effects, such as spin-valley coupling [29], Ising ferromagnetism [7], and quantum spin (anomalous) Hall effects [30,31]. In light of the recent successful growth of stanene and bismuthene and discoveries of 2D topological and superconducting phases therein [18,25,32,33], the experimental study of 2D Sn-Bi binary compounds is of crucial importance, which might offer rich material features beyond their elemental counterparts.

In this Letter, we report on the discovery of a novel 2D honeycomb structure of Sn_2Bi on a Si (111) surface. Combining scanning tunneling microscopy (STM) and

density functional theory (DFT) calculations, a honeycomb configuration is identified, in which hexagon Bi atoms are connected with each other by bonding with a triangular network of Sn atoms beneath. The scanning tunneling spectroscopy (STS) and angle-resolved photoemission spectroscopy (ARPES) measurements reveal a nearly 0.8 eV band gap. Moreover, hole gas bands in occupied states and flat band in unoccupied states are found to coexist in the same system. DFT calculations reveal that the unique honeycomb structure, where hexagon Bi atoms couple indirectly through Sn—Bi bonds, in combination with the energy-dependent hybridization between Sn and Bi results in this exotic electronic structure.

A silicon (111) wafer with a resistivity of 0.01–0.02 Ω cm was flashed to about 1250 °C to obtain a clean (7×7) reconstruction in a UHV chamber. The β phase of Si(111)-$\sqrt{3} \times \sqrt{3}$-Bi [β-Bi/Si(111) for short] was prepared by the deposition of about 1.2 monolayer (ML) Bi on a Si(111)-(7×7) surface at room temperature and subsequent annealing at 670 K [34]. To prepare honeycomb Sn_2Bi, Sn atoms were deposited on the β-Bi/Si(111) surface at 470 K. Then the sample was *in situ* transferred to the STM chamber and measured under a liquid-helium temperature. The STS were measured by a lock-in technique, in which an ac voltage of 10 mV and 676 Hz was superimposed on the tip bias. All the STM images were processed by WSxM software [35]. ARPES measurements were performed by the He Iα ($h\nu = 21.218$ eV) resonance lines and VG SCIENTA R4000 analyzer. The angular and energy resolutions were set to 0.2° and 30 meV, respectively. In the time-resolved ARPES measurements, we used 1.48-eV pump and 5.92-eV probe pulses with the repetition rate of 250 kHz. Samples were transferred *in situ* by a high-vacuum suitcase and measured at 300 K.

First-principles calculations were performed by the Vienna *ab initio* simulation package based on the density functional theory (DFT) [36], using the projector-augmented-wave potential [37], Perdew-Burke-Ernzerhof (PBE) exchange-correlation functional [38], and the plane wave basis with an energy cutoff of 250 eV. The model of the Si(111) substrate includes three Si bilayers, with the top bilayer relaxed during structural optimization and the bottom Si atoms saturated by hydrogen. A vacuum layer of ~10 Å was selected. Structural optimization was performed by applying a force convergence criterion of 0.01 eV/Å and a Gaussian smearing of 0.05 eV together with a $5 \times 5 \times 1$ Monkhorst-Pack k grid for 2×2 superstructures on Si(111). Self-consistent electronic structure calculations were done by using an $11 \times 11 \times 1$ k grid and including the SOC. STM images were simulated by the local density of states based on the Tersoff-Hamann approach [39]. The crystal structure analysis was by the particle swarm optimization (CALYPSO) algorithm [40,41].
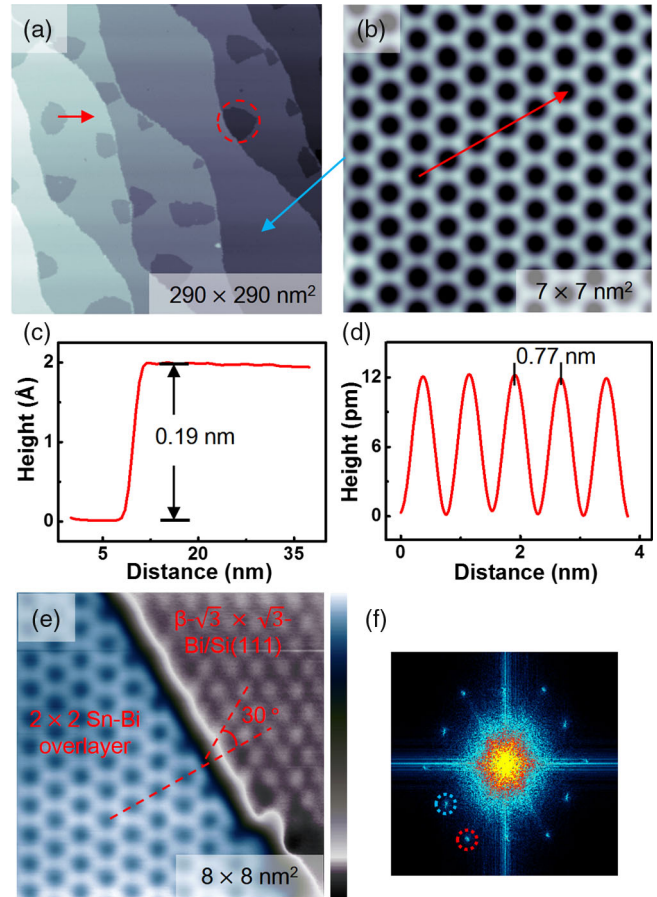

FIG. 1. A highly ordered honeycomb structure of a Sn-Bi overlayer on Si(111). (a) Large-scale STM image ($V_{\text{tip}} = -2.0$ V, $I = 90$ pA) of about 0.9 ML Sn on a β-Bi/Si(111) surface. An area of uncovered substrate is highlighted by the red dotted circle. (b) Atomic resolution STM image ($V_{\text{tip}} = 1.0$ V, $I = 90$ pA) taken on the Sn-Bi overlayer structure showing a uniform honeycomb lattice. (c) Height profile along the red arrow in (a), which indicates the height difference between the Sn-Bi overlayer and β-Bi/Si(111). (d) Line profile along the red arrow in (c). The periodicity of 0.77 ± 0.01 nm illustrates the formation of a 2×2 superstructure on Si(111). (e) Amplified STM image ($V_{\text{tip}} = 1.0$ V, $I = 99$ pA) of an area containing a boundary separating the Sn-Bi overlayer structure (bottom left) and β-Bi/Si(111) (upper right). (f) FFT patterns of a high-resolution STM image containing both a honeycomb Sn-Bi overlayer and uncovered β-Bi/Si(111). Red and blue dashed circles mark two sets of patterns that correspond to β-Bi/Si(111) and the Sn-Bi overlayer, respectively.

The deposition of Sn atoms on the β phase of a Si(111)-$\sqrt{3} \times \sqrt{3}$-Bi surface results in a uniform, highly ordered structure on the Si(111) surface as shown in the STM image in Fig. 1(a), in which the dark area is the uncovered β-Bi/Si(111) surface. A high-resolution STM image [Fig. 1(b)] shows a perfect honeycomb lattice on the terrace. The line profile [Fig. 1(d)] along the red arrow in Fig. 1(b) gives a lattice constant of 0.77 ± 0.01 nm, which is twice that of the Si(111) surface. The high-resolution
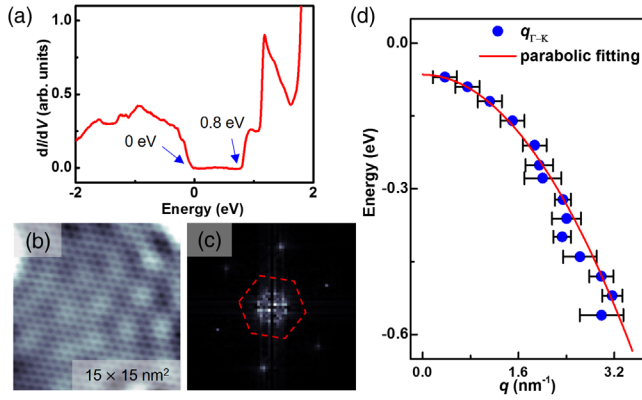
FIG. 2. Scanning tunneling spectroscopy measurements on the honeycomb structure of a Sn-Bi overlayer. (a) dI/dV spectrum taken on the Sn-Bi overlayer (initiate set point: $V_{tip} = -2$ V, $I = 400$ pA). Blue arrows mark the position of the band gap. (b) dI/dV map ($V_{tip} = 0.35$ V, $I = 250$ pA) on the Sn-Bi overlayer. (c) FFT results of (b). The first Brillouin zone is indicated by a red dashed hexagon. (d) Energy dependence of QPI wave vector q along the Γ-K direction. The data are well fitted by a red parabolic line, indicating the free-hole-like surface states.

STM image containing coexisting areas of honeycomb structure and β-Bi/Si(111) shown in Fig. 1(e) indicates that the lattice of honeycomb structures is 30° rotated with respect to the lattice of $\beta - $Bi/Si(111). Combined with the measured lattice constant of 0.77 nm, it can be concluded that the honeycomb structure is a 2×2 reconstruction with respect to the Si(111) substrate. The fast Fourier transform (FFT) of a high-resolution image including these two surface similar to the one in Fig. 1(f) also shows both 2×2 and $\sqrt{3}\times\sqrt{3}$-$R30°$ spots, corresponding to the lattices of the honeycomb structure and β-Bi/Si(111), respectively. Besides, the line profile across the boundary separating the honeycomb structure and β-Bi/Si(111) surface shown in Fig. 1(c) indicates a height difference of 0.19 ± 0.01 nm, suggesting that the honeycomb structure is about one atomic layer higher than the β-Bi/Si(111) structure.

Differential conductance (dI/dV) measurements taken on the honeycomb structure shown in Fig. 2(a) reveal a semiconducting gap of about 0.8 eV (from 0 to 0.8 eV above the Fermi level). The dI/dV maps taken at the energy range $(-0.6, 0)$ eV show clear standing-wave patterns, and an example is shown in Fig. 2(b), which contains the fluctuation of density of states (DOS) and atomic structures simultaneously. The FFT of the dI/dV map shows an isotropic circle at the center. Considering that the standing waves are due to quasiparticle interference (QPI) in the valence band, we measure the values of scattering vector q along the Γ-K direction at different energies and draw the E-q dependence in Fig. 2(d). The data can be fitted well by a parabolic curve, indicating the existence of nearly free 2D hole gas in the surface of the honeycomb structure. The fitted valence band maximum
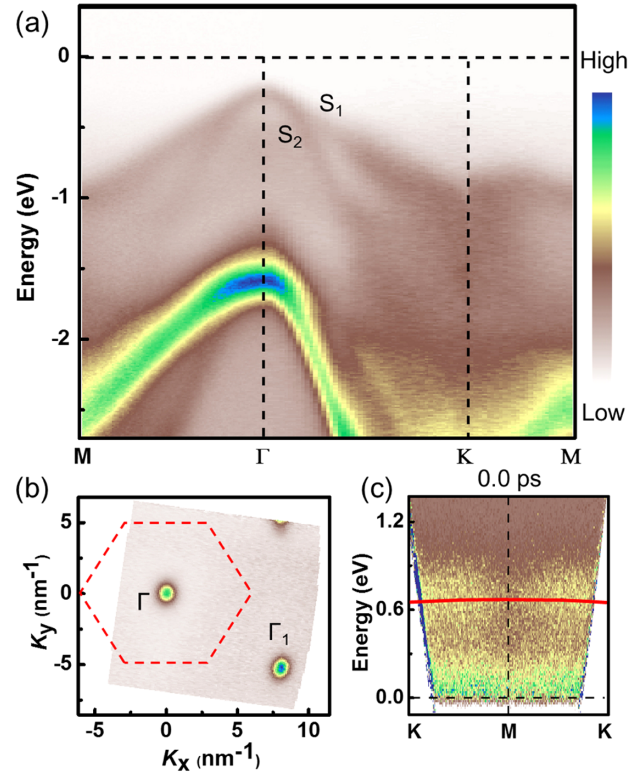

FIG. 3. Band structure of a Sn-Bi overlayer measured by ARPES. (a) Energy cut along the M-Γ-K-M direction represents two cones touching each other at the vertex below the Fermi level. (b) Constant energy contour taken at the valence band maximum (-0.2 eV). The first Brillouin zone with a red dashed hexagon is superimposed to guide the eye. (c) The bottom of the conduction band with nearly flat dispersion was observed by the pump-probe technique.

(VBM) is located at $E_0 = -65$ meV, with effective mass $m^*/m_0 = -0.14$ (m_0 is the free electron rest mass). The slightly different VBM values measured by QPI fitting and dI/dV curves (at about 0 eV) are due to the band bending induced by the STM tip [42].

To illustrate the band structure of the honeycomb lattice more explicitly, ARPES measurements were performed on a sample with 95% of the surface covered by the Sn-Bi overlayer. Band dispersions along the M-Γ-K-M directions are shown in Fig. 3(a). Two surface bands (S_1 and S_2) with the vertex overlapping at the Γ point can be distinguished unambiguously. The VBM is located at -0.2 eV (referenced to the Fermi level), which is ~ 0.2 eV lower than that in the dI/dV curve [Fig. 2(a)]. This discrepancy may arise from the photohole doping effect in ARPES and the tip-induced band bending in STS [42,43]. The constant energy contour at the VBM shows three spots in Fig. 3(b), corresponding to a 2×2 superstructure. Besides, time-resolved ARPES with a pump-probe method was performed to determine the information of unoccupied states. Interestingly, only a nearly flat band along the M-K
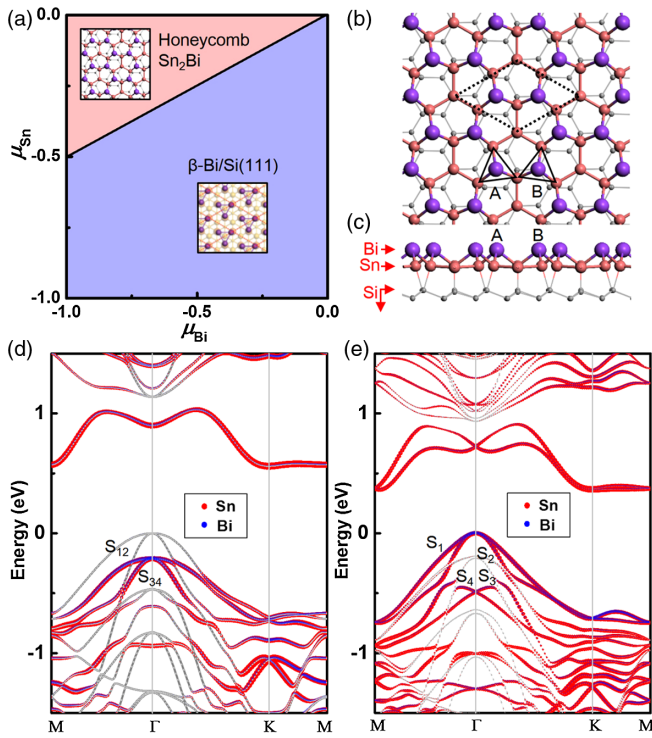
FIG. 4. Calculated phase diagram, atomic structures, and band dispersions of the honeycomb Sn_2Bi. (a) Surface phase diagram of stable Bi/Sn structures on Si(111) for varying chemical potentials of Sn (μ_{Sn}) and Bi (μ_{Bi}). μ_{Sn} (μ_{Bi}) is referenced to the Sn (Bi) bulk. (b),(c) Top and side view of the ball-and-stick model of the honeycomb Sn_2Bi, respectively. The black dashed rhombus indicates a unit cell, and two black triangles highlight the inequivalent Sn-Bi trimers. Calculated bands of the honeycomb Sn_2Bi excluding (d) and including (e) the SOC. The size of the red (blue) balls represents contributions of Sn (Bi) atoms.

direction was observed at about 0.67 eV above the Fermi level [44], as shown in Fig. 3(c).

In order to understand the atomic structure of the honeycomb Sn-Bi overlayer, we performed first-principles DFT calculations. The key issue is to find the right atomic model that can reproduce all the essential experimental results: (i) It is an atomically thin structure in a honeycomb lattice, which matches the 2×2 supercell of Si(111); (ii) it is energetically stable, to explain the high quality of the surface in both the large area and atomic scale; (iii) it gives a semiconducting band gap and a strong electron-hole asymmetry (i.e., nearly free holes and strongly localized electrons). After systematically searching for over 5000 2×2 superstructures of Si(111) with different coverages of Sn and Bi by the CALYPSO code [40,41], we obtained a surface phase diagram for varying chemical potentials of Sn and Bi in Fig. 4(a). Surprisingly, only one Sn-Bi compound phase appears in the surface phase diagram, which is energetically more favorable than β-Bi/Si(111) at Sn-rich and Bi-poor conditions (see details in Ref. [44]).

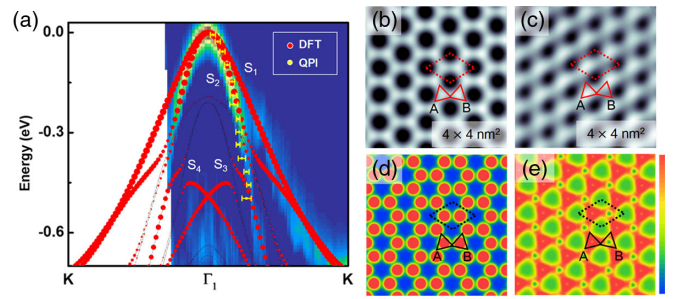This globally stable structure, named "honeycomb Sn_2Bi," gives the right atomic model as displayed in

FIG. 5. Comparison of experimental results and theoretical calculations of honeycomb Sn_2Bi. (a) Electron dispersion along the K-Γ_1-K direction from QPI measurements (yellow dots), DFT calculations (red balls), and second derivatives of ARPES data (background). (b),(c) STM images of honeycomb Sn_2Bi taken at ($V_{tip} = 1.0$ V, $I = 90$ pA) and ($V_{tip} = -1.0$ V, $I = 91$ pA). (d), (e) Simulated STM images of honeycomb Sn_2Bi taken at -1.0 eV below and $+0.46$ eV above the calculated VBM, respectively.

Figs. 4(b) and 4(c), which includes 1/2 ML Bi in the first layer and 1 ML Sn in the second layer above Si(111). The stacking geometry of Sn_2Bi/Si(111) is elaborated in Supplemental Material [44]. This structure is very stable, because all the Si, Sn, and Bi atoms satisfy the octet rule by forming four, four, and three chemical bonds, respectively. A honeycomb lattice is formed by the top Bi atoms that are located above the T_4 and H_3 sites of Si(111). The low-lying Sn atoms are either at the boundary or center of the Bi hexagon. Note that all the honeycomb Bi atoms are bridged by neighboring Sn atoms, and there is no direct bond between Bi atoms, resulting in an unusual honeycomb structure. The 2D Sn_2Bi is expected to be stable at elevated temperatures according to *ab initio* molecular dynamic simulations [44].

We make comparisons between the theory and experiments. The height difference between the honeycomb Sn_2Bi and the β-Bi/Si(111) substrate is 0.18 nm from the theory, in good agreement with the STM value of 0.19 ± 0.01 nm. Moreover, the calculated band structure [Fig. 4(e)] shows two parabolic valence bands centered at the Γ point (S_1 and S_2) and two nearly flat conduction bands minimum along the M-K direction, which are separated by an indirect semiconducting gap, consistent with the ARPES measurement. According to the determined band edges, an indirect energy gap of about 0.87 eV can be derived from the ARPES data, which is consistent with the gap value measured by STS ($\sim$0.8 eV). The theoretical gap value of 0.36 eV, typically underestimated by DFT PBE, meanwhile is comparable to the experimental value of $\sim$0.8 eV. Also, the band dispersions of S_1 and S_2 fit well with the STS measurements and ARPES data [Fig. 5(a)]. In addition, the simulated STM images [Figs. 5(d) and 5(e)] show triangular (honeycomb) patterns for unoccupied (occupied) states as observed in experiments. At the unoccupied states, the brightness contrast of the two

nearest spots in Figs. 5(c) and 5(e) can be explained by the different registry of the Bi atoms above silicon [H_3 and T_4 sites on Si(111)]. In summary, a quantitative agreement between the theory and experiments is established.

According to a band analysis, the valence and conduction bands around the Fermi level are mainly contributed by heavy elements Bi and/or Sn [Fig. 4(e)], which implies strong SOC effects in this system. The effects are emphasized by comparing band structures excluding and including the SOC [Figs. 4(d) and 4(e)]. The SOC generates a giant Rashba splitting for the lowest conduction band near the Γ point as well as a large band splitting of ~ 0.5 eV at the Γ point between the $S_{1,2}$ and $S_{3,4}$ bands. This SOC-induced band splitting can be well described by DFT PBE, as it is insensitive to material details. Indeed, ARPES observed such a kind of band splitting in Fig. 5(a); thus, the strength of the SOC of this material is experimentally quantified.

In contrast to the elemental honeycomb lattice, the Sn_2Bi binary honeycomb lattice shows a strong electron-hole asymmetry. The unique feature is inherently related to the couplings between Bi and Sn atoms. In the honeycomb structure, every Bi atom bonds to three Sn atoms to form two inequivalent trimers around a Sn atom at hollow sites. Band dispersions thus depend critically on the strength of hybridization between Bi and Sn. The hybridization is strong for the top of valence bands, which shows the character of 2D light hole gas with the effective mass $m^* = -0.14m_0$, but quite weak for the bottom of the conduction bands, leading to nearly flat bands [44]. Therefore, nearly free and strongly localized charge carriers can be both realized in the same material by tuning the Fermi level.

Electrons in a dispersionless flat band with quenched kinetic energy are highly degenerate, which provides an ideal platform to realize the strongly correlated electronic states. In 2D materials, flat bands are predicted theoretically in square (lieb) lattices [53,54], kagome lattices [55,56], and honeycomb (hexagonal) lattices [57,58] but observed only on some artificial systems [54]. By tuning the Fermi level of the novel 2D system, transport measurements in flat bands may bring surprising properties like ferromagnetism and superconductivity [59,60]. Furthermore, the nearly free-hole-like carriers in the S_1 and S_2 bands with spin splitting indicate that the 2D Sn_2Bi with a semiconducting gap will be a good candidate for high-performance nanoelectronic devices.

Like $Sn_2Bi/Si(111)$, similar 2D materials X_2Y (X = group IVA, Y = group VA) could be grown on substrates that satisfy the conditions of surface lattices commensurate with that of the 2D overlayer, small lattice mismatch, and one-electron dangling bond per surface site. Candidate substrates include (111) surfaces of rhombohedral and cubic structures as well as (001) surfaces of hexagonal structures. For instance, we expect that the 2D Sn_2Bi could be grown on Ge(111) and ZnS(111). This offers opportunities to explore new 2D binary compounds and novel quantum phenomena.

J. G., B. X., and H. Li contributed equally to this work.

[*]yongxu@mail.tsinghua.edu.cn
[†]khwu@iphy.ac.cn
[‡]lchen@iphy.ac.cn

[1] K. S. Novoselov, A. K. Geim, S. V. Morozov, D. Jiang, M. I. Katsnelson, I. V. Grigorieva, S. V. Dubonos, and A. A. Firsov, Nature (London) 438, 197 (2005).

[2] K. S. Novoselov, A. K. Geim, S. V. Morozov, D. Jiang, Y. Zhang, S. V. Dubonos, I. V. Grigorieva, and A. A. Firsov, Science 306, 666 (2004).

[3] B. A. Bernevig, T. L. Hughes, and S.-C. Zhang, Science 314, 1757 (2006).

[4] M. König, S. Wiedmann, C. Brüne, A. Roth, H. Buhmann, L. W. Molenkamp, X.-L. Qi, and S.-C. Zhang, Science 318, 766 (2007).

[5] C.-Z. Chang et al., Science 340, 167 (2013).

[6] C. Gong et al., Nature (London) 546, 265 (2017).

[7] B. Huang et al., Nature (London) 546, 270 (2017).

[8] K. Chang et al., Science 353, 274 (2016).

[9] X. Xi, L. Zhao, Z. Wang, H. Berger, L. Forro, J. Shan, and K. F. Mak, Nat. Nanotechnol. 10, 765 (2015).

[10] Y. Saito, T. Nojima, and Y. Iwasa, Nat. Rev. Mater. 2, 16094 (2016).

[11] Q. H. Wang, K. Kalantar-Zadeh, A. Kis, J. N. Coleman, and M. S. Strano, Nat. Nanotechnol. 7, 699 (2012).

[12] D. Malko, C. Neiss, F. Vines, and A. Gorling, Phys. Rev. Lett. 108, 086804 (2012).

[13] B. Feng, Z. Ding, S. Meng, Y. Yao, X. He, P. Cheng, L. Chen, and K. Wu, Nano Lett. 12, 3507 (2012).

[14] A. Fleurence, R. Friedlein, T. Ozaki, H. Kawai, Y. Wang, and Y. Yamada-Takamura, Phys. Rev. Lett. **108**, 245501 (2012).

[15] D. Chiappe, E. Scalise, E. Cinquanta, C. Grazianetti, B. van den Broek, M. Fanciulli, M. Houssa, and A. Molle, Adv. Mater. **26**, 2096 (2014).

[16] M. Derivaz, D. Dentel, R. Stephan, M. C. Hanf, A. Mehdaoui, P. Sonnet, and C. Pirri, Nano Lett. **15**, 2510 (2015).

[17] L. Zhang, P. Bampoulis, A. N. Rudenko, Q. Yao, A. van Houselt, B. Poelsema, M. I. Katsnelson, and H. J. W. Zandvliet, Phys. Rev. Lett. **116**, 256804 (2016).

[18] F. F. Zhu, W. J. Chen, Y. Xu, C. L. Gao, D. D. Guan, C. H. Liu, D. Qian, S. C. Zhang, and J. F. Jia, Nat. Mater. **14**, 1020 (2015).

[19] A. Molle, J. Goldberger, M. Houssa, Y. Xu, S. C. Zhang, and D. Akinwande, Nat. Mater. **16**, 163 (2017).

[20] B. Feng, J. Zhang, Q. Zhong, W. Li, S. Li, H. Li, P. Cheng, S. Meng, L. Chen, and K. Wu, Nat. Chem. **8**, 563 (2016).

[21] A. J. Mannix *et al.*, Science **350**, 1513 (2015).

[22] C. Gu *et al.*, ACS Nano **11**, 4943 (2017).

[23] J. L. Zhang *et al.*, Nano Lett. **16**, 4903 (2016).

[24] X. Wu *et al.*, Adv. Mater. **29**, 1605407 (2017).

[25] F. Reis, G. Li, L. Dudy, M. Bauernfeind, S. Glass, W. Hanke, R. Thomale, J. Schafer, and R. Claessen, Science **357**, 287 (2017).

[26] V. O. Ozcelik, K. Gong, and C. E. White, Nano Lett. **18**, 1786 (2018).

[27] V. O. Ozcelik, S. Cahangirov, and S. Ciraci, Phys. Rev. Lett. **112**, 246803 (2014).

[28] Z. Gao, X. Dong, N. Li, and J. Ren, Nano Lett. **17**, 772 (2017).

[29] J. R. Schaibley, H. Yu, G. Clark, P. Rivera, J. S. Ross, K. L. Seyler, W. Yao, and X. Xu, Nat. Rev. Mater. **1**, 16055 (2016).

[30] F. D. M. Haldane, Phys. Rev. Lett. **61**, 2015 (1988).

[31] C. L. Kane and E. J. Mele, Phys. Rev. Lett. **95**, 226801 (2005).

[32] Y. Xu, B. Yan, H. J. Zhang, J. Wang, G. Xu, P. Tang, W. Duan, and S. C. Zhang, Phys. Rev. Lett. **111**, 136804 (2013).

[33] M. Liao *et al.*, Nat. Phys. **14**, 344 (2018).

[34] T. Kuzumaki, T. Shirasawa, S. Mizuno, N. Ueno, H. Tochihara, and K. Sakamoto, Surf. Sci. **604**, 1044 (2010).

[35] I. Horcas, R. Fernandez, J. M. Gomez-Rodriguez, J. Colchero, J. Gomez-Herrero, and A. M. Baro, Rev. Sci. Instrum. **78**, 013705 (2007).

[36] G. Kresse and J. Furthmüller, Phys. Rev. B **54**, 11169 (1996).

[37] G. Kresse and D. Joubert, Phys. Rev. B **59**, 1758 (1999).

[38] J. P. Perdew, K. Burke, and M. Ernzerhof, Phys. Rev. Lett. **77**, 3865 (1996).

[39] J. Tersoff and D. R. Hamann, Phys. Rev. B **31**, 805 (1985).

[40] Y. Wang, J. Lv, L. Zhu, and Y. Ma, Phys. Rev. B **82**, 094116 (2010).

[41] Y. Wang, J. Lv, L. Zhu, and Y. Ma, Comput. Phys. Commun. **183**, 2063 (2012).

[42] R. M. Feenstra, J. Vac. Sci. Technol. B **21**, 2080 (2003).

[43] Y. Terada, S. Yoshida, A. Okubo, K. Kanazawa, M. Xu, O. Takeuchi, and H. Shigekawa, Nano Lett. **8**, 3577 (2008).

[44] See Supplemental Material at http://link.aps.org/supplemental/10.1103/PhysRevLett.121.126801 for the detail of atomic structure determination, energy-dependent Sn-Bi hybridization analysis, and ARPES measurement, which includes Refs. [42,45–52].

[45] Y. Ohtsubo, P. LeFevre, F. Bertran, and A. Taleb-Ibrahimi, Phys. Rev. Lett. **111**, 216401 (2013).

[46] Y. Kohsaka, T. Machida, K. Iwaya, M. Kanou, T. Hanaguri, and T. Sasagawa, Phys. Rev. B **95**, 115307 (2017).

[47] C. Yamanouchi, K. Mizuguchi, and W. Sasaki, J. Phys. Soc. Jpn. **22**, 859 (1967).

[48] K. Sakamoto *et al.*, Phys. Rev. Lett. **103**, 156801 (2009).

[49] J. Myslivećek, F. Dvořák, A. Stróżecka, and B. Voigtländer, Phys. Rev. B **81**, 245427 (2010).

[50] S. Nosé, Mol. Phys. **52**, 255 (1984).

[51] W. G. Hoover, Phys. Rev. A **31**, 1695 (1985).

[52] K. Reuter and M. Scheffler, Phys. Rev. B **65**, 035406 (2001).

[53] K. Sun, Z. Gu, H. Katsura, and S. Das Sarma, Phys. Rev. Lett. **106**, 236803 (2011).

[54] M. R. Slot, T. S. Gardenier, P. H. Jacobse, G. C. P. van Miert, S. N. Kempkes, S. J. M. Zevenhuizen, C. M. Smith, D. Vanmaekelbergh, and I. Swart, Nat. Phys. **13**, 672 (2017).

[55] E. Ohgushi, S. Murakami, and N. Nagaosa, Phys. Rev. B **62**, R6065 (2000).

[56] E. Tang, J. W. Mei, and X. G. Wen, Phys. Rev. Lett. **106**, 236802 (2011).

[57] C. Wu, D. Bergman, L. Balents, and S. Das Sarma, Phys. Rev. Lett. **99**, 070401 (2007).

[58] W. Beugeling, J. C. Everts, and C. M. Smith, Phys. Rev. B **86**, 195129 (2012).

[59] A. Mielke, Phys. Rev. Lett. **82**, 4312 (1999).

[60] Z. X. Shen and D. S. Dessau, Phys. Rep. **253**, 1 (1995).